Simulation of the Fertilization Ca^{2+} Wave in *Xenopus laevis* Eggs

John Wagner,* Yue-Xian Li,* John Pearson,§ and Joel Keizer*#
*Institute of Theoretical Dynamics and #Section on Neurobiology, Physiology and Behavior, University of California, Davis, California 95616 and §Applied Theoretical and Computational Physics, Los Alamos National Laboratory, Los Alamos, New Mexico 87545

ABSTRACT In the preceding paper Fontanilla and Nuccitelli (*Biophysical Journal* 75:2079–2087 (1998)) present detailed measurements of the shape and speed of the fertilization Ca^{2+} wave in *Xenopus laevis* eggs. In order to help interpret their results, we develop here a computational technique based on the finite element method that allows us to carry out realistic simulations of the fertilization wave. Our simulations support the hypothesis that the physiological state of the mature egg is *bistable*, i.e., that its cytoplasm can accommodate two alternative physiological Ca^{2+} concentrations: a low concentration characteristic of the prefertilization state and a greatly elevated concentration characteristic of the state following the passage of the wave. We explore this hypothesis by assuming that the bistability is due to the release and re-uptake properties of the endoplasmic reticulum (ER) as determined by inositol trisphosphate (IP_3) receptor/Ca^{2+} channels and sarcoendoplasmic reticulum calcium ATPase (SERCA) pumps. When combined with buffered diffusion of Ca^{2+} in the cytoplasm, our simulations show that inhomogeneities in the Ca^{2+} release properties near the plasma membrane are required to explain the temporal and spatial dependences of the shape and speed of these waves. Our results are consistent with an elevated IP_3 concentration near the plasma membrane in the unfertilized egg that is augmented significantly near the site of fertilization. These gradients are essential in determining the concave shape of the Ca^{2+} fertilization wave front.

INTRODUCTION

Twenty-one years ago Ridgeway et al. (1997) reported that free calcium increases explosively in activating *Medaka* eggs. In the intervening years sperm-induced Ca^{2+} signals have been observed in eggs of species ranging from starfish and frog to hamster and human (Nuccitelli, 1991; Taylor et al., 1993). Although the nature of the Ca^{2+} signal is different for different species, it usually spreads as a wave of intracellular Ca^{2+} that emanates from the point of sperm-egg fusion (Jaffe, 1991). These waves are an integral part of egg activation and appear to be involved in initiation of key processes in the embryonic cell cycle.

Fertilization in the African frog, *Xenopus laevis*, induces a Ca^{2+} wave that travels across the egg like a slow tidal wave, moving at a speed of 5–10 $\mu m\ s^{-1}$ (Nuccitelli et al., 1993). In a paper in this issue, Fontanilla and Nuccitelli (1998) report the first detailed measurements of this wave made from deep within the egg. These measurements provide time-resolved, fluorescent-ratioed confocal images of the Ca^{2+} wave as it moves across the equatorial plane separating the animal and vegetal hemispheres of the egg. By arranging the egg such that fertilization occurs preferentially in the equatorial plane, the authors capture images that provide a reproducible two-dimensional slice through the three-dimensional Ca^{2+} wave. Their measurements show that the equatorial plane of the egg is symmetric about the axis through the two hemispheres. This permits analysis of the shape and speed of the wave front as a function of position and time since the shape and speed are independent of the point of sperm fusion.

A number of detailed features of the Ca^{2+} wave emerge from these and previous experiments (Nuccitelli et al., 1993). First, the wave propagates like a tide, with basal cytosolic calcium $[Ca^{2+}]_i$ of the order of 0.2–0.3 μM in front of the wave and 1.3–2.0 μM in its wake. Second, the wave initiates as a thin crescent in the cortex at the site of fertilization. Third, the wave propagates with a concave shape until it reaches the opposite side of the egg. Fourth, the wave front is relatively sharp ($\sim$ 50 μm) with a rise time of the order of 10–20 s. Fifth, $[Ca^{2+}]_i$ is higher in the cortical region both before and after fertilization and overshoots its value in the wake. And sixth, the wave speed varies along the wave front with higher speeds in the cortical region.

In an effort to understand these features of the fertilization wave in *Xenopus*, we have carried out simulations of the propagation of the wave in two dimensions in a circular domain. The fact that the wave propagates as a tide suggests that it arises from a *bistable* physiological state of Ca^{2+} in the cytoplasm. According to this idea the Ca^{2+} handling mechanisms in the mature egg can support two alternative physiological Ca^{2+} concentrations, a low basal concentration typical of the prefertilization state and an elevated concentration typical of Ca^{2+} behind the wave. Bistability is a well known phenomenon in both reactive chemical solutions and electrical circuits and is associated with hysteresis (Goldbeter, 1996; Keizer et al., 1995a). Bistability has recently been used to describe maturation of the immature *X. laevis* oocyte (Ferrell and Machleder, 1998)

Here we pursue the notion that the bistability of $[Ca^{2+}]_i$ in the mature *Xenopus* egg is caused by the same underlying

Received for publication 18 March 1998 and in final form 17 June 1998.
Address reprint requests to Dr. Joel E. Keizer, Institute of Theoretical Dynamics, Section on Neurobiology, Physiology and Behavior, University of California, Davis, CA 95616. Tel.: 530-752-0938; Fax: 530-752-7297; E-mail: jekeizer@ucdavis.edu.

0006-3495/98/10/2088/10 $2.00

mechanisms responsible for spiral waves in immature *Xenopus* eggs. Both mature and immature *Xenopus* eggs are known to possess active inositol 1,4,5-trisphosphate receptors (IP_3R). The IP_3R is a Ca^{2+} release channel residing in the ER (Berridge, 1993) and is known to be regulated by both IP_3 and Ca^{2+} (Bezprozvanny et al., 1991; Keizer et al., 1995b; Watras et al., 1991). Previous theoretical work has shown that the spiral waves can be generated in the immature oocyte by release of Ca^{2+} from the ER stores via the IP_3R in combination with refilling of the stores by SERCA type ATPases (Atri et al., 1993; Jafri and Keizer, 1995), and it is plausible that the IP_3R is involved in setting the bistable state of cytoplasmic Ca^{2+} in *X. laevis* eggs.

The most puzzling of the experimental observations is that the shape of the wave front is concave. To explain this observation and the fact that $[Ca^{2+}]_i$ is elevated in the cortex before fertilization requires three things: first, that the rate of Ca^{2+} release in the cortex of the egg is greater than that in the center before fertilization; second, that fertilization induces a further increase in Ca^{2+} release rate that is localized to the cortical region near the site of attachment; and third, that the fertilization-induced Ca^{2+} release rate involves a gradient in the release rate with a maximum that extends along the cortical region from the site of sperm attachment. This third feature is essential for explaining the slender crescent shape of the initial wave front. In our simulations, these inhomogeneities in the $[Ca^{2+}]_i$ release rate are achieved using local gradients in the concentration of IP_3.

The simulations presented here have several novel features. They are the first calculations of Ca^{2+} waves in *Xenopus* oocytes that use a realistic boundary shape (circular) with boundary conditions that are appropriate to the cell type (no Ca^{2+} flux) (cf. Schaff et al. (1997) for a neuroblastoma cell). This has been accomplished by using a finite element numerical scheme to integrate the differential equations. As we discuss in the following sections, an adequate treatment of the cell surface is essential for interpreting the experimental observations of Fontanilla and Nuccitelli (1998). One of the main conclusions from our simulations is that the shape of the Ca^{2+} wave front helps reveal physiological inhomogeneities in the egg, and quite probably in other cells as well. We are currently extending this method to three dimensions in order to perform even more realisic simulations of the fertilization wave.

PHYSIOLOGICAL MODELING AND METHODS

Our modeling has two important goals: (1) to develop a minimal computational model based on available physiological data for the local Ca^{2+} handling mechanisms in *Xenopus* oocytes and (2) to develop numerical methods for efficient computation of waves in a realistic geometry, including inhomogeneities. As a first step we focus here on explaining the origin of the concave shape of the fertilization Ca^{2+} wave front.

By incorporating specific assumptions about the uptake and release mechanism in the egg our simulations test several hypotheses. The first is that Ca^{2+} in the cytoplasm of the mature *Xenopus* egg is in a bistable physiological state. This is suggested by the character of the observed wave, which involves an abrupt transition of $[Ca^{2+}]_i$ from a low to an elevated value that remains high for an extended period of time. Taken by itself, this observation does not exclude the possibility that the cytoplasm becomes bistable after fertilization. Thus the Ca^{2+} wave might be preceded by a wave of IP_3 initiated by sperm fusion that transforms the cytoplasm into a bistable state. However, the fact that other stimuli (e.g., microinjection of Ca^{2+} (Nuccitelli et al., 1993) and IP_3 (Busa et al., 1985) can also initiate a similar Ca^{2+} wave suggests that bistability is a consequence of maturation. Further evidence favoring formation of a bistable egg before fertilization comes from the existence of a threshold Ca^{2+} concentration below which additions of Ca^{2+} fail to initiate a wave (Nuccitelli et al., 1993). This type of threshold behavior is a hallmark of bistability.

Our second hypothesis is that IP_3R channels and SERCA pumps are the dominant Ca^{2+} handling mechanism involved in the generation and propagation of the fertilization Ca^{2+} wave. This is based on the observations that in *Xenopus* oocytes: (1) ryanodine channels appear to be absent (Parys et al., 1992); (2) IP_3 is required for the propagation of Ca^{2+} waves (DeLisle and Welsh, 1992); and (3) addition of heparin inhibits the fertilization wave in *Xenopus* as does inhibition of phosphatidylinositol bisphosphate (PIP_2) hydrolysis (Nuccitelli et al., 1993; Fontanilla and Nuccitelli, 1998). Single channel measurements of the open probability of the IP_3R (Bezprozvanny et al., 1991; Watras et al., 1991) have shown that while IP_3 potentiates Ca^{2+} release, cytosolic Ca^{2+} regulates the channel opening in a bell-shaped manner, activating opening when $[Ca^{2+}]_i$ increases up to a threshold $[Ca^{2+}]_i$ value and inactivating opening when $[Ca^{2+}]_i$ increases beyond the threshold. Other experiments also demonstrate the $[Ca^{2+}]_i$ dependence of the IP_3R channel activity (Iino, 1990; Parys et al., 1992), with activation occurring rapidly and inactivation slowly (Finch et al., 1991; Parker and Ivorra, 1990). We incorporate these key features of regulation of the IP_3R into our simulations.

The second hypothesis can be translated into differential equations (cf. Eqs. A1 and A2) like those used previously to explain IP_3-induced $[Ca^{2+}]_i$ oscillations (De Young and Keizer, 1992; Li and Rinzel, 1994). When combined with diffusion of Ca^{2+} in the cytosol (Atri et al., 1993; Jafri and Keizer, 1995), the equation for $[Ca^{2+}]_i$ involves a balance of three terms:

$$\frac{\partial [Ca^{2+}]_i}{\partial t} = J_{rel} - J_{fil} + D_{eff}\nabla^2[Ca^{2+}]_i \qquad (1)$$

Here the rate of Ca^{2+} release from the ER through IP_3 channels and leaks is denoted by J_{rel}, while J_{fil} denotes the rate of Ca^{2+} influx into the ER via SERCA-type ATPase Ca^{2+} pumps. The final term in Eq. 1 is due to Ca^{2+} diffusion, with D_{eff} the effective (buffered) diffusion coefficient of Ca^{2+} in the cytosolic space. This balance equation provides a concise quantitative representation of how Ca^{2+} uptake and release by the ER and diffusion in the cytosol determine $[Ca^{2+}]_i$ changes in space and time.

The change in the physiological state of the cytoplasm of the *Xenopus* egg from one that supports $[Ca^{2+}]_i$ oscillations and spiral waves, as observed in the immature oocyte (Lechleiter and Clapham, 1992), to one that supports only a traveling wave front, as found in the egg (Fontanilla and Nuccitelli, 1998), can be understood by a shift in balance between J_{rel} and J_{fil}. Fig. 1 illustrates one possible scenario leading to a bistable state with only the release properties of the IP_3R being altered. In both states the solid sigmoid curve gives the dependence of J_{fil} on $[Ca^{2+}]_i$. The bell-shaped curves, on the other hand, represent the dependence of the release flux J_{rel} on $[Ca^{2+}]_i$ and are typical of that measured experimentally. The bell shape is caused by the biphasic regulation of the IP_3R by $[Ca^{2+}]_i$. When the peak of the bell curve is shifted to the left (dotted line), it can explain spiral waves in the immature *Xenopus* oocyte (Atri et al., 1993; Jafri and Keizer, 1995). On the other hand, by lowering the affinity of the IP_3R for $[Ca^{2+}]_i$, the bell-shaped curve shifts to the right (dashed line). This relatively small change is sufficient to make the physiological state of the cytoplasm bistable.

This change in state can be understood by examining the steady state Ca^{2+} levels that are determined by Eq. 1. Setting the left hand side of Eq. 1 equal to 0 and neglecting diffusion, $[Ca^{2+}]_i$ is seen to be steady only when $J_{rel} = J_{fil}$. The values of $[Ca^{2+}]_i$ at which this occurs can be found by looking for the intersections of the the sigmoidal J_{fil} curve with the

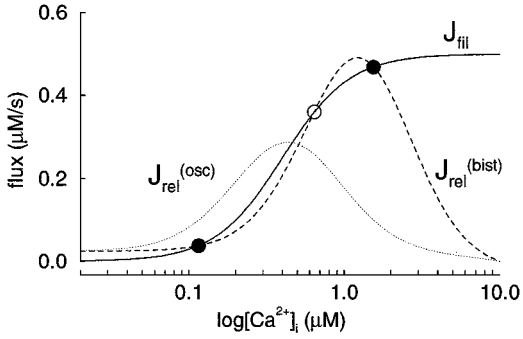

FIGURE 1 Bistability resulting from the balance between the Ca^{2+} release and uptake by the ER. The rate of $[Ca^{2+}]_i$ influx into the ER via SERCA pumps, J_{fil}, is plotted as a function of $[Ca^{2+}]_i$ (*solid line*) along with the rate of Ca^{2+} release efflux, J_{rel}(osc), that produces oscillations (*dotted line*), and the altered rate, J_{rel}(bist), that produces bistability (*dashed line*). The parameter values used are in Table 1 in the Appendix except that for the dotted line $d_{act} = 0.6$ μM and $d_{inh} = 0.5$ μM.

bell-shaped J_{rel} curve in Fig. 1. The bell-shaped curve on the left intersects J_{fil} exactly once, yielding a single steady state. That steady state, however, can be shown to be unstable (De Young and Keizer, 1992) and leads to Ca^{2+} oscillations. However, when the release curve is shifted to the right, three intersections occur. It is easy to show that the state in the center, indicated by the open circle, is unstable, whereas the high and low $[Ca^{2+}]_i$ states (filled circles) are stable. The existence of these two very different stable physiological states means that the cytoplasm is bistable (Goldbeter, 1996).

Although it is known in certain cells that the properties of the IP_3R can be modulated by phosphorylation (Marshall and Taylor, 1993) and that even IP_3 itself can shift the bell-shaped activity of the IP_3R to the left (Kaftan et al., 1997), it is not known if this occurs in *Xenopus* oocytes. Nonetheless, for simplicity we adopt this mechanism to explain the bistability of the cytoplasm in the mature egg. Calculations described in the Appendix were carried out first in one spatial dimension to insure that the planar wave speed and wave width were comparable to those observed by Fontanilla and Nuccitelli (1998). In the remaining sections we explore what additional properties of the release and filling mechanisms contribute to the shape of the wave front.

RESULTS

The cytoplasm of the *Xenopus* egg is known to be partitioned into regions with distinct physiological characteristics, e.g., the animal and vegetal hemispheres and the cortex (Gilbert, 1994). However, we focus here on the shape of the wave front in the equatorial plane separating the two hemispheres. Fontanilla and Nuccitelli's (1998) data show that the properties of this plane are symmetric about the axis through the two hemispheres. Thus we first examine the shape of the fertilization wave when our two-dimensional simulation slice is homogeneous, i.e., when all of the parameters in the model are the same throughout the slice. In subsequent sections we examine how inhomogeneities, which still have this axial symmetry, alter the shape of the wave front. In all of the calculations we have assumed no-flux boundary conditions. This is in line with (1) the experimental observation that removal of Ca^{2+} from the external medium does not significantly alter the properties of the wave (Fontanilla and Nuccitelli, 1998) and (2) the fact that significant Ca^{2+} efflux would favor a convex wave front near the membrane.

Wave fronts in a homogeneous cytoplasm

The upper panel of Fig. 2 *A* shows a simulated wave in a small (25 μm diameter) egg at four time points. The wave is initated at time $t = 0$ with a small localized increase of Ca^{2+} at the site of fertilization. As the wave traverses the egg, the wave front is first convex, flattens roughly halfway across, and becomes concave in the second half, terminating at a point at the far side. In these simulations the wave front always intersects perpendicular to the boundary, as required by the imposed no-flux condition at the membrane. Fig. 2 *B* shows the simulated time course of $[Ca^{2+}]_i$ at the 18 points indicated by the triangles (cortex) and squares (center) in the lower panel of Fig. 2 *A*. The large initial values of $[Ca^{2+}]_i$ at the first few points reflect the increase in $[Ca^{2+}]_i$ required to initiate the wave. To compare with experiment (Fontanilla and Nuccitelli, 1998), Fig. 2 *C* plots the wave speed at points along the center of the egg (squares) and the cortex (triangles). Note that in both regions the wave speed increases as the front progresses across the egg.

In Fig. 2, the wave front changes gradually from convex (negative curvature) to concave (positive curvature) even in the cortical region. Simulation results with other small-diameter cells are qualitatively similar and differ significantly from the shape of the wave in *Xenopus*, which is concave throughout (Fontanilla and Nuccitelli, 1998). Moreover, experimentally the wave speed is greatest in the cortex near the fertilization site, which is not the case in these simulations.

To test whether the shape and speed of the wave front are due only to the small size of the simulated cell, we carried out comparable calculations for larger cell sizes. Fig. 3 shows typical results for a 1.0-mm diameter egg. As in the smaller egg, the Ca^{2+}-initiated wave propagates initially with a convex front. However, the front remains convex throughout the entire cell, becoming concave just before reaching the other side (not shown). Fig. 3 *B* again shows $[Ca^{2+}]_i$ as a function of time at points through the cortex (upper plot) and in the center (lower plot). Note that as the wave propagates across the egg, peak $[Ca^{2+}]_i$ increases more in the cortical region than through the center. The fact that $[Ca^{2+}]_i$ is higher in the cortex is due to the no-flux boundary, which restricts diffusion of Ca^{2+}. This effect is also evident in Fig. 3 *C*, which plots the wave speed in the cortex and at the center. The speed again increases monotonically, achieving a maximum at the far side of the egg. Thus cell size does not explain the shape and speed of the wave front in *Xenopus*.

The wave in Fig. 3 was initiated by a localized $[Ca^{2+}]_i$ elevation at the fertilization site. Since the shape of the wave front might also be influenced by how the wave is initiated, we tried initiating the wave with a $[Ca^{2+}]_i$ elevation that was restricted to the cortical region at the site of fertiliza-

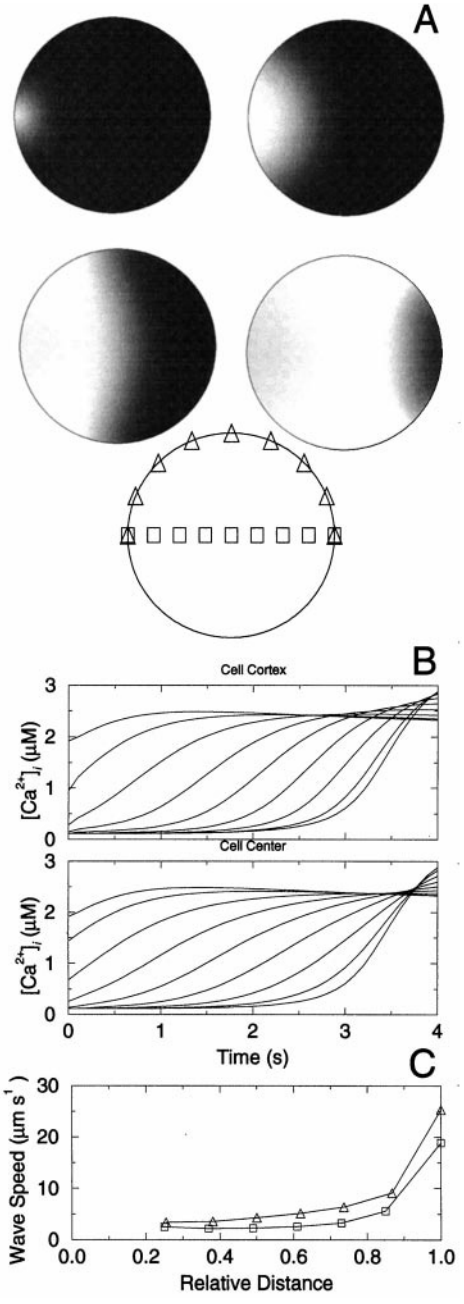

FIGURE 2 Simulated fertilization wave in an small (25 μm diameter), homogeneous egg initiated by a localized elevation of $[Ca^{2+}]_i$ near the point of sperm fusion. (*A*) The $[Ca^{2+}]_i$ profile represented as successive gray-scale images at $t = 0.5$, 1.5, 2.5, and 3.0 s. (*B*) Time series of $[Ca^{2+}]_i$ in the cortex (triangles) or center (squares) of the cell as indicated in the lower image of 2 *A*. The abcissa represents the relative distance from the fertilization site either along the cortex or the center of the cell. (*C*) Variation in wave speed at the locations indicated in the lower image of 2 *A*. Wave speed in this and other figures calculated from the distance between ajacent points centered at either the squares (center) or triangles (cortex) divided by the time taken for the half maximum of the wave front to traverse that distance. Parameter values are as in Table 1 of the Appendix. Gray-scale range is 0.0 μM $[Ca^{2+}]_i$ = black, 2.0 μM $[Ca^{2+}]_i$ = white.

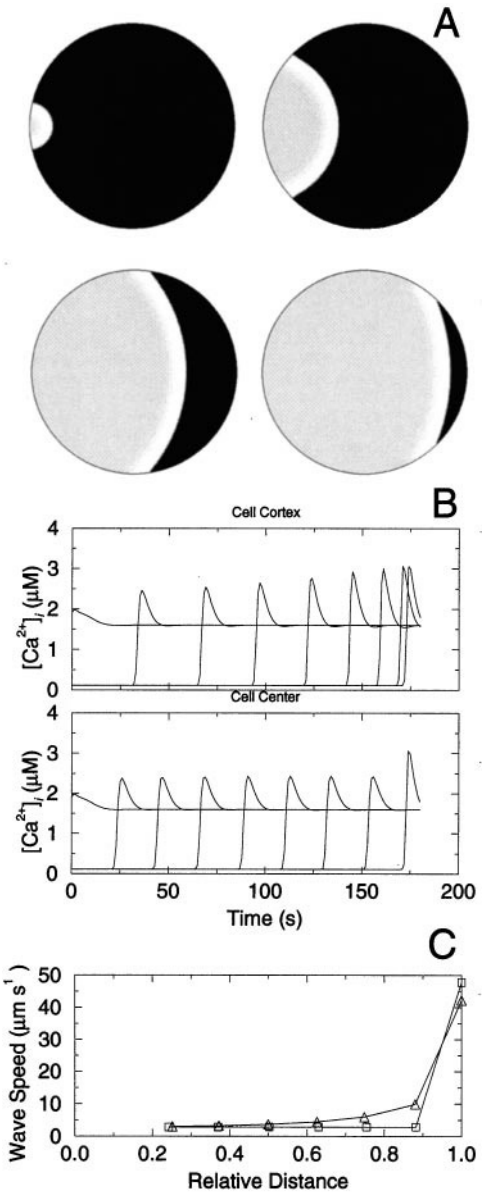

FIGURE 3 Simulated fertilization wave in a 1.0 mm diameter, homogeneous egg. (*A*) Gray scale images of $[Ca^{2+}]_i$ initiated by the same $[Ca^{2+}]_i$ elevation as in Fig. 2 at $t = 20$, 60, 120, and 160 s. (*B*) Time series of $[Ca^{2+}]_i$ variations sampled at the center and the cortex (cf. Fig. 2 *B*). (*C*) The speed of wave front through the center (*squares*) and in the cortex (*triangles*) calculated as in panel 2 *C*. Parameter values are given in Table 1 of the Appendix. Gray scale is same as Fig. 2 *A*. Because of the large diameter of the cell, the slight curvature that makes the wave front perpendicular at the boundary (due to absense of flux at the boundary) is difficult to see in the gray scale image.

tion. This did not help reproduce the typical concave shape of the wave in *Xenopus* nor the sharp wave front in the cortical region. The lack of success with simulations using a homogeneous egg suggested that the characteristic concave shape of the front might be due to inhomogeneities of the cytoplasmic medium.

Inhomogeneities and wave front profiles

We have investigated the influence of two types of cytoplasmic inhomogeneities on the wave front: radially sym-

metric inhomogeneities and inhomogeneities localized at the site of fertilization. We have carried out numerous simulations in which various parameters of the model (Table 1 and Appendix) were distributed radially. These included the fraction of free Ca^{2+} in the cytosol (β), the overall rate of Ca^{2+} uptake and release (λ), the inactivation time of the IP_3R (τ_0), and the diffusion constant of Ca^{2+} (D). Although inhomogeneous distributions of these parameters give reasonable wave shapes in the second half of the cell (not shown), they give a convex shape initially. Thus these features of Ca^{2+} handling do not seem to be candidates for the inhomogeneity.

As discussed in the Appendix, altering β, λ, τ_0, and D does not alter the balance of the ER Ca^{2+} release rate, J_{rel}, and the ER Ca^{2+} filling rate, J_{fil}. Consequently, we explored the possibility of increasing J_{rel} relative to J_{fil} in the cortical region. This has the additional advantage of increasing the value of $[Ca^{2+}]_i$ in the cortical region under basal conditions, in line with the results of Fontanilla and Nuccitelli (1998). One way to achieve this is to increase the relative density of the IP_3R in the cortical region by decreasing v_p (see Appendix). However, we have found that the most effective mechanism for increasing wave speed in the cortical region and achieving concave wave shapes similar to experiment involves gradients of IP_3: first, a higher concentration of IP_3 at the plasma membrane before fertilization; and second, a significant tangential gradient of IP_3 near the site of fertilization.

The justification for using such gradients is the localized production of IP_3 at the plasma membrane followed by its diffusion into the interior of the cell where it degrades (Allbritton et al., 1992). Fig. 4 *A* shows an axially symmetric distribution of IP_3 that is twice as high at the plasma membrane, simulating a increased rate of production of IP_3 there. To correspond with the experimental observations that show elevated values of $[Ca^{2+}]_i$ localized in the neighborhood of the cortex (Fontanilla and Nuccitelli, 1998), we have increased the concentration of IP_3 appreciably only within the first 15–20 μm of the plasma membrane. This increases the value of J_{fil} in the cortex and elevates cortical $[Ca^{2+}]_i$ before fertilization by about 10%, as also shown in Fig. 4 *A*. By itself, this radially symmetric distribution of IP_3 does not lead to a Ca^{2+} wave that is initially convex. This is remedied, however, if the concentration of IP_3 is increased near the site of fertilization. Fig. 4 *B* illustrates the combined distributions in the upper left quadrant of the equatorial plane. For emphasis, the restricted grey scale image shows high IP_3 concentrations as black with the maximum value of $[IP_3]$ at the fertilization site equal to 0.96 μM. This combined distribution can initiate a wave *without* independently increasing $[Ca^{2+}]_i$.

We have carried out simulations with the symmetric distribution of IP_3 shown in Fig. 4 *A*, first initiating the wave as in Figs. 2 and 3 with a localized increase of $[Ca^{2+}]_i$

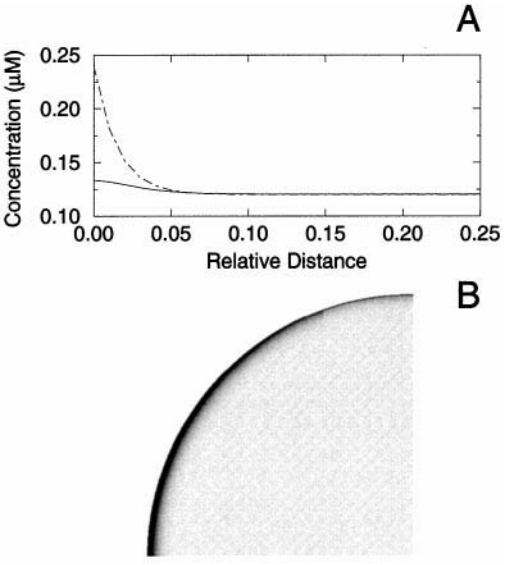

FIGURE 4 (*A*) Radial inhomogeneity of IP_3 distribution used in simulations in Figs. 5 and 6 (*dashed line*) along with the radial dependence of the resulting steady $[Ca^{2+}]_i$ distribution (*solid line*). The abcissa is the relative radial distance from the plasma membrane. The radial distribution of IP_3 has the form:

$$[IP_3](r) = I_s(1 + I_h\exp[((r/r_c) - 1)/I_w])$$

where $I_s = 0.12$ μM, $I_h = 1.0$, $I_w = 0.015$;

$r_c = 0.5$ mm is the radius of the cell and r is radial distance from the cell surface. (*B*) Gray-scale image of the IP_3 distribution in panel *A* added to the tangential distribution:

$$[IP_3](r) = I_h'\exp[((r/r_c) - 1)/I_w]\exp[-(y/I_w'r_c)^4]\text{step}(-(x + x^*))$$

with $I_h' = 0.84$ μM, $I_w' = 0.8$, $x^* = 167$ μm, step(x) = 1 for $x \geq 0$ and

= 0 for $x < 0$;

(x, y) is the Cartesian coordinate of a point in the egg with (0,0) at the center; other quantities defined in Fig. 4 *B*. Gray scale is 0.1 μM = white, 0.5 μM = black. The greatest elevation of the combined distribution is at the fertilization site, where $[IP_3] = 0.96$ μM; $[IP_3] = 0.12$ μM in the cell center.

TABLE 1 Parameter values and initial conditions

Parameter value	
v_L	$5 \cdot 10^{-4}$
d_I	0.025 μM
k_p	0.4 μM
v_P	0.1 μM
I_s	0.12 μM
C_{er}	10 μM
τ_0	4 s
d_{act}	1.2 μM
D	300 $\mu m^2 s^{-1}$
λ	112.5 s^{-1}
d_{inh}	1.5 μM
β	0.053
Initial conditions	
$C(0) = 0.1153$ μM	
$h(0) = 0.93$	

at the site of fertilization. No matter how large the egg, this does not produce a concave shape of the wave front. A typical simulation for a 1.0-mm diameter egg is shown in Fig. 5, which shows a wave nearly identical to that in Fig. 3. The problem is that the gradient of IP_3 is perpendicular to the plasma membrane. Although this increases cortical $[Ca^{2+}]_i$ before fertilization and the wave speed perpendicular to the boundary, it does not increase it tangentially, i.e., along the cortex.

To achieve an increase of wave speed in the tangential direction, we have had to include tangential gradients of IP_3 like that in Fig. 4 *B*. Figure 6 shows simulations initiated exclusively by that additional gradient. Fig. 6 *A* shows the wave profile at six time points as the wave traverses a 1.0-mm diameter egg. In this simulation the wave is first seen (top left image; $t = 25$ s) as a thin crescent centered at the site of fertilization that spreads rapidly in the cortical direction (top right image; $t = 30$ s). Unlike the waves initiated by $[Ca^{2+}]_i$, there is a substantial delay (~ 25 s) from the time that the tangential component of IP_3 is established to the time the wave is first visible. As the wave traverses the cell, the front tends to flatten and develops small bumps reminiscent of the detailed structure of the front in the experimental images (Fontanilla and Nuccitelli, 1998). Moreover, the front retains its overall concave shape across the entire cell. The details in the structure of the wave front are dependent on the exact functional form assumed for the tangential IP_3 gradient. Nonetheless, the initial crescent and concave shape of the wave front require only a sufficient concentration of IP_3 to trigger release and the existence of a significant gradient tangential to the membrane.

Fig. 6 *B* shows $[Ca^{2+}]_i$ as a function of time at points through the cortex (upper panel) and in the center (lower panel). As before, calcium is higher in the cortex than in the center (by 20–30%) with a minimum in the cortex about halfway across the cell. This is due to the additional IP_3 gradient, which declines in the cortex. Effects of the IP_3 gradient are also evident in Fig. 6 *C*, where the wave speed

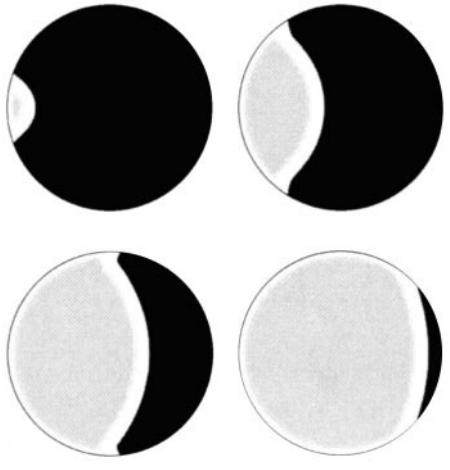

FIGURE 5 Simulated fertilization wave in a 1.0-mm diameter egg with elevated IP_3 in the cortical region (Fig. 4) and initiated by a localized elevation of $[Ca^{2+}]_i$ near the point of sperm fusion. The $[Ca^{2+}]_i$ profile represented as successive gray scale images at $t = 20$, 80, 120, and 180 s. Gray scale is the same as in Fig. 2.

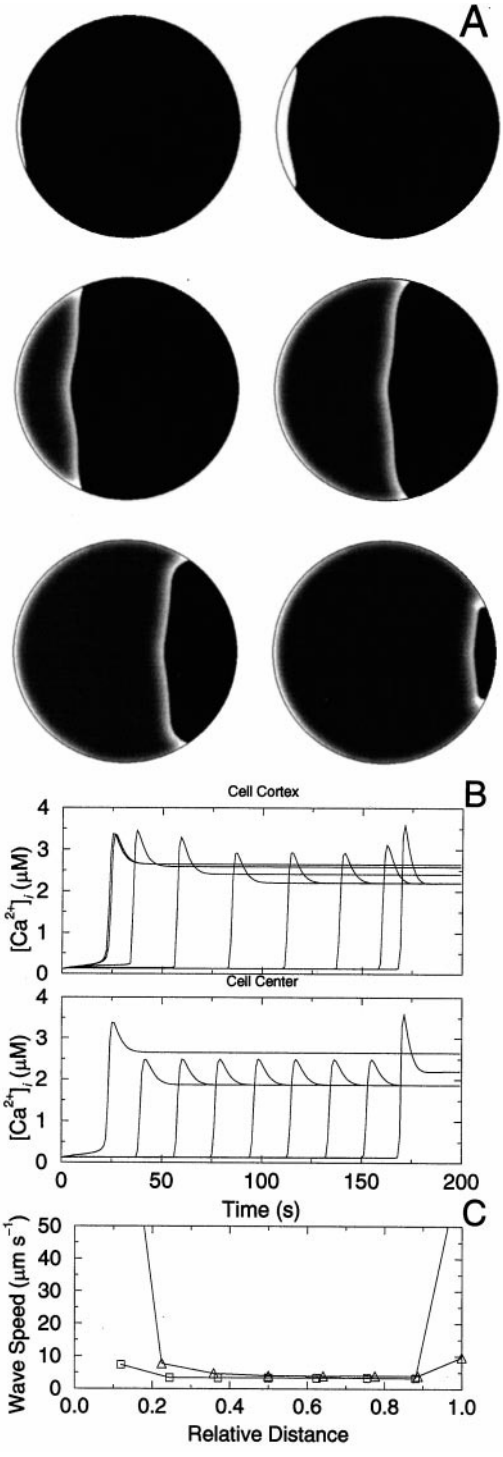

FIGURE 6 Simulated fertilization wave in a 1.0-mm diameter egg with IP_3 elevated radially as in Fig. 4 *A* and initiated by a tangential gradient of IP_3 in the cortical region (Fig. 4 *B*). Parameters are as in Table 1, except $D_{eff} = 20\ \mu m^2 s^{-1}$ and $\lambda = 250$. (*A*) Restricted gray scale images of $[Ca^{2+}]_i$ at $t = 25$, 30, 60, 100, 125, and 160 s. Gray scale is $[Ca^{2+}]_i \leq 1.6\ \mu M$ = black, $[Ca^{2+}]_i \geq 2.6\ \mu M$ = white. (*B*) Time series of $[Ca^{2+}]_i$ as in Fig. 3 *B*. (*C*) Wave speed as in Fig. 3 *C*.

through the center of the egg (squares) and in the cortex (triangles) is plotted. Through the center the decreasing rate of Ca^{2+} release due to decreasing concentration of IP_3 is stronger than the curvature effect on these waves (Tyson and Keener, 1988), causing the wave to slow down as it moves toward the center of the egg. As the wave moves through the second half of the egg, the wave speed increases again as the concentration of IP_3 increases. When initiated with IP_3 as in Fig. 6, the wave travels down an IP_3 gradient in the cortical region. This leads to a decline in peak $[Ca^{2+}]_i$ in the cortex as well as a decline in $[Ca^{2+}]_i$ in the cortical wake. After the wave passes through the initial IP_3 distribution, peak $[Ca^{2+}]_i$ increases due to the curvature of the boundary, which blocks Ca^{2+} from diffusing away from the wave front.

To enhance the structure of the Ca^{2+} gradient behind the wave front, Fig. 6 uses a restricted gray-scale map with all values of $[Ca^{2+}]_i$ below 1.6 μM and above 2.6 μM assigned the same gray-scale values. It is clear from this image that at the wave front cortical $[Ca^{2+}]_i$ is much higher than in the center of the egg. This is particularly noticeable in the final frame, where the bright region in the cortex is similar to that seen in the fluorescent images of Fontanilla and Nuccitelli (1998).

SUMMARY AND DISCUSSION

Relying on the experimental measurements of Fontanilla and Nuccitelli (1998) for comparison, we have used computer simulations to investigate the shape and speed of the fertilization Ca^{2+} wave in *X. laevis* eggs. Existing experimental evidence suggests that the fertilization wave is caused by release of Ca^{2+} from the ER via IP_3R Ca^{2+} channels (Nuccitelli *et al*, 1993). Release of Ca^{2+} from these channels is potentiated by IP_3 and both activated and inhibited by Ca^{2+} (Kaftan et al., 1997; Keizer et al., 1995b; Marshall and Taylor, 1993). We have used these facts to construct a minimal model of Ca^{2+} handling in *Xenopus* eggs that exhibits the property of bistability, i.e., the simultaneous existence of low and high Ca^{2+} concentration states of the cytoplasm. The bistable model leads to Ca^{2+} waves in one spatial dimension that move as a slow tide across the cell with wave speeds comparable to those measured experimentally. When these simulations are repeated in a circular disk to mimic the two-dimensional geometry of a confocal slice, the shape of the wave front is found to be convex, rather than concave as is observed experimentally. Indeed, a wave front with a concave shape cannot be obtained in this geometry if the Ca^{2+} handling properties of the cytoplasm are assumed to be spatially uniform.

The concave shape of the wave front implies that the wave moves faster tangentially to the plasma membrane, i.e., around the cortex, than through the center of the egg. This suggests that Ca^{2+} handling properties in the cortex of the egg differ from those deeper inside the cell. Indeed, it is known that the density of the cortical ER increases during maturation of the oocyte (Charbonneau and Grey, 1984; Campanella et al., 1994) and that the plasma membrane is rich in PIP_2 (Snow et al., 1996), the substrate for production of IP_3 via phospholipase C (Marshall and Taylor, 1993). Other inhomogeneities may exist as well, including localization of Ca^{2+} buffers and SERCA pumps. On the other hand, a role for influx of external Ca^{2+} at the plasma membrane has been ruled out experimentally (Fontanilla and Nuccitelli, 1998).

We have simulated a variety of inhomogeneities to see if they can explain the increased speed of the wave in the cortical region of the cell and the convex shape of the wave front. The most successful of these simulations (cf. Fig. 6) have used a radially symmetric increase of IP_3 in the cortical region that mimics the production of IP_3 at the plasma membrane along with an additional increase of IP_3 localized to the fertilization site. The local increase of IP_3 at the fertilization site simulates a sperm-induced production of IP_3, perhaps via a tyrosine kinase (Yim et al., 1994). Depending on the extent of buffering of IP_3 by binding sites and its turnover by the IP_3 3-kinase and 5-phosphatase (Sims and Allbritton, 1998), it is plausible that diffusion, degradation, and localized production of IP_3 at the plasma membrane are sufficient to produce a static distribution of the size used in the simulations.

It is important that this additional IP_3 have a tangential gradient, i.e., that it decrease as the distance from the fertilization site increases along the cortex. In addition, the concentration of IP_3 near the fertilization site must be sufficient to initiate the wave. Although this increases the Ca^{2+} gradient tangential to the plasma membrane, it is not the Ca^{2+} gradient that is responsible for the initial crescent shape in our simulations. Rather, the shape and rapid expansion of the crescent (Fig. 6 *A*, top images) are due to sequential releases of Ca^{2+} around the cortex caused by the tangential gradient in IP_3. Moving away from the fertilization site along the cortex, the concentration of IP_3 declines, giving rise to longer delay times for the initial releases of Ca^{2+}. Thus the rapid initial speed of the cortical wave (Fig. 6 *C*) does not involve diffusion of Ca^{2+}, implying that the initial crescent propagates as a kinematic wave (Jafri and Keizer, 1994, 1995). Without the increased tangential component of IP_3, the speed of the cortical wave front is not fast enough to produce the overall concave shape of the wave.

The simulations reported here have been designed to investigate whether bistability and inhomogeneities in Ca^{2+} release mechanisms in the *Xenopus* egg can explain the shape of the wave front. They are based, however, on only a semiquantitative understanding of the regulation of the IP_3 in the mature *Xenopus* egg. The parameters in the model have been set to produce bistability with the low concentration state at 0.11 μM and the high Ca^{2+} concentration state in the range of 1.5−2.0 μM. This leads to tides with plateau values of $[Ca^{2+}]_i$ that are higher by a factor of 1.5–2 than those deduced from the confocal fluorescence (Fontanilla and Nuccitelli, 1998). By altering parameters it should be possible to adjust the plateau values of $[Ca^{2+}]_i$

closer to those estimated experimentally. However, due to the simplifications present in the model, we have not attempted to do this. The present simulations reproduce a number of other features seen in the fluorescence-time records. These include elevated cortical $[Ca^{2+}]_i$ before fertilization; the rise time of the wave front (order of 10–20 s); the initial overshoot of $[Ca^{2+}]_i$ in the cortex; and the decline of the peak value of $[Ca^{2+}]_i$ to a long-lasting plateau. Our simulations also reproduce the relative values of $[Ca^{2+}]_i$ in the measured time courses. For example, the peak and plateau of $[Ca^{2+}]_i$ in the cortex near the fertilization site exceeds that near the center of the cell (cf. Fig. 6 *B*). Our results also mimic the observed elevation of $[Ca^{2+}]_i$ in the cortical region compared to the center of the egg. Fontanilla and Nuccitelli (1998) report that experimentally, the average value of $[Ca^{2+}]_i$ during the wave is about 70% higher in the cortex than in the center of the egg and about 15% higher in the unfertilized egg. In our simulations this is explained by the inhomogeneous distribution of IP_3 localized near the plasma membrane.

We believe that our simulations argue strongly in favor of bistability as the dynamic mechanism underlying the fertilization Ca^{2+} wave in *Xenopus* eggs. We think they also lend credence to the hypothesis that an inhomogenous distribution of Ca^{2+} handling mechanisms due to local gradients of IP_3 are important in determining the shape of the wave. On the other hand, our simulations are limited by the facts that (1) they involve only two spatial dimensions; (2) they ignore the effect of Ca^{2+} depletion of the ER (Jafri and Keizer, 1995); (3) they do not include diffusion, production, and degradation of IP_3 explicitly; (4) they do not include the potential influence of mitochondrial Ca^{2+} handling (Jouaville et al., 1995), which plays a significant role in other cells types when $[Ca^{2+}]_i$ exceeds about 0.5–0.7 μM (Babcock et al., 1997); and (5) possible remodeling of the ER after passage of the Ca^{2+} wave (Terasaki et al., 1996) is not included. Remodeling of the ER might help explain the slow decline of $[Ca^{2+}]_i$ after the wave has crossed the cell, which cannot be explained with the present model. We have recently modified our simulations to overcome the first three limitations; the results substantiate the conclusions reached with the simpler model presented here and will be reported in a future communication.

APPENDIX

Equations and parameters

Simulations were carried out using two partial differential equations. These equations are based on the De Young-Keizer model for gating of the IP_3R by $[Ca^{2+}]_i$ and IP_3 (De Young and Keizer, 1992), as simplified by Li and Rinzel (1994) and Atri et al. (1993):

$$\frac{1}{\beta}\frac{\partial C}{\partial t} = \lambda\left[\left(v_L + \left(\frac{I}{I+d_I}\right)^3\left(\frac{C}{C+d_{act}}\right)^3 h^3\right)(C_{er} - C) - v_P\frac{C^2}{C^2+k_P^2}\right] + D\nabla^2 C \quad \text{(A1)}$$

$$\frac{dh}{dt} = (d_{inh} - (C + d_{inh})h)/\tau_0 \quad \text{(A2)}$$

Here C and C_{er} represent $[Ca^{2+}]_i$ and ER Ca^{2+}, respectively; h, which varies between 0 and 1, is the fraction of IP_3 channels not inactivated by Ca^{2+}; and I denotes the intracellular IP_3 concentration. These equations are a continuum approximation to the cytoplasmic milieu, in which the ER and cytosolic compartments occupy a given volume fraction of the cytoplasm at each point in space. Because the ER is highly reticulated and extends continuously through out the entire cytoplasmic space (Terasaki et al., 1994), this is a good approximation on lengths scales greater than a few micrometers. For simplicity, Eqs. A1 and A2 neglect the influence of depletion of the ER and diffusion of Ca^{2+} in the ER on the release rate.

The first term on the right hand side of Eq. A1, J_{rel}, gives the rate of Ca^{2+} release from the ER, while the second term, J_{fil}, describes the rate of Ca^{2+} uptake into the ER through SERCA pumps. The parameter β denotes the fraction of Ca^{2+} that is not bound to buffers in the cytosol (Wagner and Keizer, 1994), and λ scales the density of IP_3R channels and SERCA pumps in the ER membrane. The Ca^{2+} diffusion constant in the absence of buffer is indicated by D and the effective diffusion constant in buffered medium is $D_{eff} = \beta D$ (Wagner and Keizer, 1994). We have chosen a standard value of $\beta = 0.053$, to give a value $D_{eff} = 16\ \mu m^2\ s^{-1}$, which is of the order of that measured in the *Xenopus* oocyte (Allbritton et al., 1992). The characteristic time for $[Ca^{2+}]_i$-dependent inactivation of the IP_3R is τ_0. Changes in the buffering capacity (β), λ, τ_0, and the diffusion constant of Ca^{2+} (D) do not alter the steady states in Fig. 1, which are determined by the balance between J_{rel} and J_{fil}. On the other hand, changing τ_0 can change the stability of the steady states.

The parameter d_{act} defines the Ca^{2+} concentration associated with activation of the open probability (the bell-shaped curve in Fig. 1) whereas d_{inh} is the characteristic Ca^{2+} concentration for inhibition. In order to achieve bistability, it is necessary that the value of d_{act} be larger than the value that produces oscillations, shifting the bell-shaped curve to the right as shown in Fig. 1. Although the phenomenon of bistability is robust for small changes in d_{act}, the model has only a single steady (or oscillatory) state if d_{act} is much smaller or larger than the value $d_{act} = 1.2\ \mu M$ in Table 2 unless other parameters are also changed. Our simulations use $d_{inh} = 1.5\ \mu M$, which produces a low $[Ca^{2+}]_i$ steady state value in the range of 0.1 μM and a high Ca^{2+} value of the order of 2 μM. Simulations are not terribly sensitive to this parameter, except that for $d_{inh} < 1.25\ \mu M$ the system is no longer bistable and for values of $d_{inh} > 2.0\ \mu M$, $[Ca^{2+}]_i$ in the upper state becomes unphysiologically high.

To assist in finding appropriate values of β, λ, and I, we have explored how these parameters effect the wave speed, v, and width of the wave front, ω by simulating Eqs. A1 and A2 in one spatial dimension. Simulations were carried out on a 1.0-mm line with no-flux boundary conditions at the end points. Waves were initiated by a localized elevation of $[Ca^{2+}]_i$ at one end, which created a traveling wave front with a fixed speed. The width of the wave front was determined as the product of the wave speed and the time required for $[Ca^{2+}]_i$ to increase from 5% to 95% of its maximum value during the passage of the front. Results of the simulations, along with the value of the parameters chosen for the two-dimensional simulations, are shown in Fig. 7 *A-C*. The parameter values and initial conditions used in the simulations are given in Table 1 unless specified otherwise in the figure legends.

Computational methods

Numerical computations were performed using a "finite difference in time, finite element in space" Galerkin formulation of the finite element method (Douglas and Dupont, 1970; Zienkiewicz, 1977) using linear basis functions and triangular (T_3) elements ranging in area from 3.8 to 15.6 μm^2. The circular domain was constructed by first triangulating a square domain, and then deleting triangles whose centers fell outside the circle; the resulting boundary nodes were then adjusted to the circle boundary, and nearest-neighbor averaging of nodes was performed to decrease variability in triangle areas. We used a fixed time step, which was reduced until

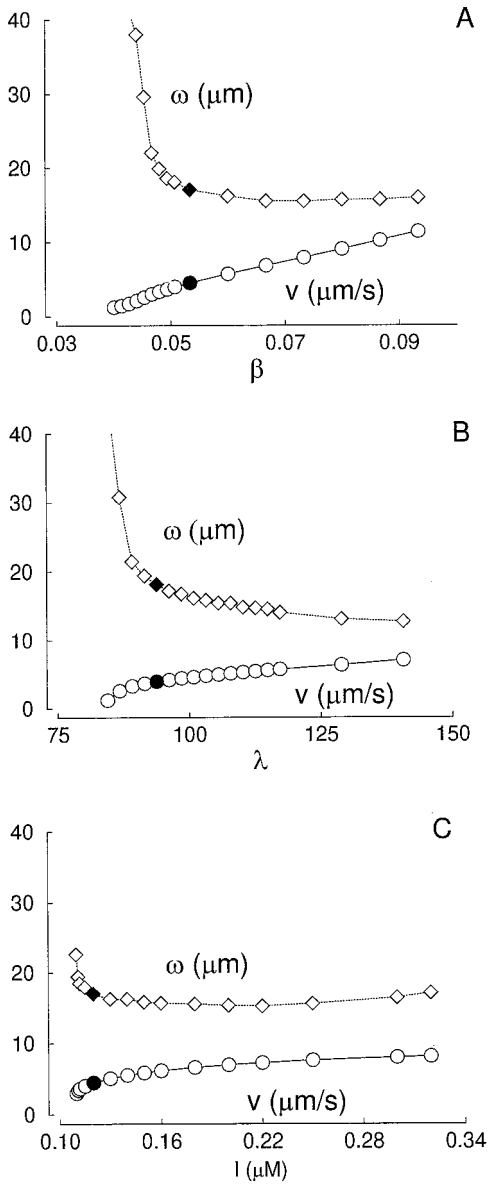

FIGURE 7 (*A-C*) Wave speed, v, and front width, ω, as a function of parameters β, λ, and I based on simulations of Eqs. A1 and A2 in one spatial dimension. The open circles represent the wave speed and the open diamonds denote the width of the wave front. The filled circles and diamonds correspond to parameter values used in the other two panels; other parameters as in Table 1, except $d_I = 0.03$ μM.

further reductions produced no significant changes in the results; these steps were typically between 0.1 and 0.25 s. At each time step, the discretized equations were solved iteratively using successive over-relaxation (SOR), with a convergence criterion of 10^{-8} using a discrete L_2 norm. A detailed description of the finite element approach and mesh generation techniques is reported elsewhere (Wagner, 1998).

The method was validated by testing the code in several ways. First, the basis function representation in the finite element approximation was tested by representing known functions on the mesh. Second, the code was used to solve the heat-diffusion equation on the mesh, both for transient and steady state conditions with zero flux at the boundaries. Third, the accuracy of the no-flux boundary condition was checked using total mass balance for the domain. Finally, the code was used to solve problems with the diffusion coefficient set to 0 and the results compared to solutions generated with the Runge-Kutta method. The combined results of these tests suggest that the simulations reported here are accurate to at least three significant figures.

We thank our experimental collaborators, Richard Nuccitelli and Ray Fontanilla, for numerous conversations and advice during the course of this work.

This work was supported by National Institutes of Health Grant RR10081 and by the Agricultural Experiment Station of the University of California at Davis.

REFERENCES

Allbritton, N., T. Meyer, and L. Stryer. 1992. Range of messenger action of calcium ion and inositol 1,4,5-trisphosphate. *Science*. 258: 1812–1815.

Atri, A., J. Amundson, D. Clapham, and J. Sneyd. 1993. A single pool model for intracellular calcium oscillations and waves in the *Xenopus laevis* oocyte. *Biophys. J.* 65:1727–1739.

Babcock, D. F., J. Herrington, P. C. Goodwin, Y. B. Park, and B. Hille. 1997. Mitochondrial participation in the intracellular Ca^{2+} network. *J. Cell Biol.* 136:833–844.

Berridge, M. J. 1993. Inositol trisphosphate and calcium signalling. *Nature.* 361:315–325.

Bezprozvanny, I., J. Watras, and B. E. Ehrlich. 1991. Bell-shaped calcium response curves of Ins(1, 4, 5)P_3- and calcium-gated channels from endoplasmic reticulum of cerebellum. *Nature).* 351:751–754.

Busa, W. B., J. E. Ferguson, S. K. Joseph, J. R. Williamson, and R. Nuccitelli. 1985. Activation of frog (*Xenopus laevis*) eggs by inositol trisphosphate I: characterization of Ca^{2+} release from intracellular stores. *J. Cell Biol.* 101:677–682.

Campanella, C., P. Andreucceti, C. Taddei, and R. Talevi. 1984. The modifications of cortical endoplasmic reticulum during in vitro maturation of *Xenopus laevis* oocytes and its involvement in cortical granule exocytosis. *J. Exp. Zool.* 229:283–293.

Charbonneau, M., and R. Grey. 1984. The onset of activation responsiveness during maturation coindices with the formation of the cortical endoplasmic reticulum in oocytes of *Xenopus laevis*. *Dev. Biol.* 102: 90–97.

DeLisle, S. and M. J. Welsh. 1992. Inositol trisphosphate is required for the propagation of calcium waves in *Xenopus* oocytes. *J. Biol. Chem.* 267:7963–7966.

De Young, G. and J. Keizer. 1992. A single-pool inositol 1,4,5-trisphosphate-receptor-based model for agonist-stimulated oscillations in Ca^{2+} concentration *Proc. Natl. Acad. Sci. USA.* 89:9895–9899.

Douglas, J. Jr., and T. Dupont. 1970. Galerkin methods for parabolic equations. *SIAM J. Numer. Anal.* 7:575–626.

Ferrell, J. E. Jr., and E. M. Machleder. 1998. The biochemical basis of an all-or-none cell fate switch in *Xenopus* oocytes. *Science.* 280:895–898.

Finch, E. A., T. J. Turner, and S. M. Goldin. 1991. Calcium as a coagonist of inositol 1,4,5-trisphosphate-induced calcium release. *Science.* 252: 443–446.

Fontanilla, R. A., and R. Nuccitelli. 1998. Characterization of the sperm-induced calcium wave in *Xenopus* eggs using confocal microscopy, *Biophys. J.* 75:2079–2087.

Gilbert, F. S. 1994. Developmental Biology, 4th edition. Sinauer, Sunderland, MA. Chap. 4.

Goldbeter, A. 1996. Biochemical Oscillations and Cellular Rhythms. Cambridge University Press, Cambridge. 91.

Iino, M. 1990. Biphasic Ca^{2+}-dependence of inositiol 1,4,5-trisphosphate-induced Ca^{2+} release in smooth muscle cells of the guinea pig Taenia caeci. *J. Gen. Physiol.* 95:1103–1122.

Jaffe, L. F. 1991. The path of calcium in calcium oscillations: a unifying hypothesis. *Proc. Natl. Acad. Sci. USA.* 88:9883–9887.

Jafri, S., and J. Keizer. 1994. Diffusion of inositol 1,4,5-trisphosphate, but not Ca^{2+}, is necessary for a class of inositol 1,4,5-trisphosphate-induced Ca^{2+} waves. *Proc. Natl. Acad. Sci. USA.* 91:9485–9489.

Jafri, S., and J. Keizer. 1995. On the roles of Ca^{2+} diffusion, Ca^{2+} buffers, and the endoplasmic reticulum in IP_3 -induced Ca^{2+} waves. *Biophys. J.* 69:2139–2153.

Jouaville, L. S., F. Ichas, E. L. Holmuhamedov, P. Camacho, and J. D. Lechleiter. 1995. Synchronization of calcium waves by mitochondrial substrates in *Xenopus laevis* oocytes. *Nature.* 337:438–441.

Kaftan, E. J., B. E. Ehrlich, and J. Watras. 1997. Inositol 1,4,5-trisphosphate ($InsP_3$) and calcium interact to increase the dynamic range of $InsP_3$ receptor-dependent calcium signaling. *J. Gen. Physiol.* 110: 529–538.

Keizer, J., L. W. Maki, G. D. Smith, and J. P. Bruinsma. 1995a. Bistability and fluctuations for an incandescent light bulb. *J. Phys. Chem.* 99: 844–852.

Keizer, J., Y.-L. Li, J. Rinzel, and S. Stojilković. 1995b. $InsP_3$-induced Ca^{2+} excitability of the endoplasmic reticulum. *Mol. Biol. Cell.* 6:945–951.

Lechleiter, J. D., and D. Clapham. 1992. Molecular mechanisms of intracellular calcium excitability in *X. laevis* oocytes. *Cell.* 69:283–294.

Li, Y.-X., and J. Rinzel. 1994. Equations for $InsP_3$ receptor-mediated $[Ca^{2+}]_i$ oscillations derived from a detailed kinetic model: a Hodgkin-Huxley like formalism. *J. Theor. Biol.* 166:461–473.

Marshall, I. C. B., and C. W. Taylor. 1993. Regulation of inositol 1,4,5-trisphosphate receptors. *J. Exp. Biol.* 184:161–182.

Murray, J. D. 1989. Mathematical Biology. Springer-Verlag, Berlin. 232–238.

Nuccitelli, R. 1991. How do sperm activate eggs? *Curr. Top. Dev. Biol.* 25:1–16.

Nuccitelli, R., D. L. Yim, and T. Smart. 1993. The sperm-induced Ca^{2+} wave following fertilization of the *Xenopus* egg requires the productions of $Ins(1, 4, 5)P_3$. *Dev. Biol.* 158:200–212.

Parker, I., and I. Ivorra. 1990. Inhibition by Ca^{2+} of inositol trisphosphate-mediated Ca^{2+} liberation: a possible mechanism for oscillatory release of Ca^{2+}. *Proc. Natl. Acad. Sci. USA.* 87:260–264.

Parys, J. B., S. W. Sernett, S. DeLisle, P. M. Snyder, M. J. Welsh, and K. P. Campbell. 1992. Isolation, characterization, and localization of inositol 1,4,5-trisphosphate receptor protein in *Xenopus laevis* oocytes. *J. Biol. Chem.* 267:18776–18782.

Ridgeway, E. B., J. C. Gilkey, and L. F. Jaffe. 1977. Free calcium increases explosively in activating *Medaka* eggs. *Proc. Natl. Acad. Sci. USA.* 74:623–627.

Schaff J., C. C. Fink, B.Slepchenko, J. H. Carson, and L. M. Loew. 1997. A general computational framework for modeling cellular structure and function. *Biophys. J.* 73:1135–1146.

Sims, C. E., and N. L. Allbritton. 1998. Metabolism of inositol 1,4,5-trisphosphate and inositol 1,3,4,5-tetrakisphosphate by the oocytes of *Xenopus laevis*. *J. Biol. Chem.* 273:4052–4058.

Snow, P., D. L. Yim, J. D. Leibow, S. Saini, and R. Nuccitelli. 1996. Fertilization stimulates an increase in inositol trisphosphate and inositol lipid levels in *Xenopus* eggs. *Dev. Biol.* 180:108–118.

Taylor, C. T., Y. M. Lawrence, C. R. Kingsland, M. M. Biljan, and K. S. R. Cuthbertson. 1993. Oscillations in intracellular free calcium induced by spermatozoa in human oocytes at fertilization. *Hum. Reprod.* 8:2174–2179.

Terasaki, M., N. T. Slater, A. Fein, A. Schmidek, and T. S. Reese. 1994. Continuous network of endoplasmic reticulum in cerebellar Purkinje neurons. *Proc. Natl. Acad. Sci. USA.* 91:7510–7514.

Terasaki, M., L. A. Jaffe, G. R. Hunnicutt, and J. A. Hammer, III. 1996. Structural change of the endoplasmic reticulum during fertilization: evidence for loss of membrane continuity using the green fluorescent protein. *Dev. Biol.* 179:320–328.

Tyson, J., and J. P. Keener. 1988. Singular pertubation theory of travelling waves in excitable media. *Physica D.* 32:327–361.

Wagner, J., and J. Keizer. 1994. Effects of rapid buffers on Ca^{2+} oscillations. *Biophys. J.* 67:447–456.

Wagner, J. 1998. A mathematical model of the fertilization Ca^{2+} wave in the *Xenopus laevis* egg. Doctoral Thesis. University of California, Davis.

Watras, J., I. Bezprozvanny, and B. E. Ehrlich. 1991. Inositol 1,4,5-trisphosphate-gated channels in cerebellum: presence of multiple conductance states. *J. Neurosci.* 11:3239–3245.

Yim, D. L., L. K. Opresko, H. S. Wiley, and R. Nuccitelli. 1994. Highly polarized EGF receptor tyrosine kinase activity initiates egg activation in *Xenopus*. *Dev. Biol.* 162:41–55.

Zienkiewicz, O. C. 1977. The Finite Element Method. 3rd ed. McGraw-Hill, London.